

## Development of Regression Models for the Prediction of NiTi Archwire Forces in an Orthodontic Bracket System Using Response Surface Methodology

Sareh Aiman Hilmi Abu Seman, Ching Wei Ng, Muhammad Fauzinizam Razali\*  
and Abdus Samad Mahmud

*School of Mechanical Engineering, Engineering Campus, Universiti Sains Malaysia, 14300 USM, Nibong Tebal, Pulau Pinang, Malaysia*

### ABSTRACT

Superelastic NiTi archwire is extensively employed in the early stage of orthodontic therapy due to its capacity to transmit constant and light force to the tooth. The archwire force prediction for orthodontic treatment planning becomes a challenging process as the generated friction at the wire-bracket interface modifies the force exerted by the NiTi archwire. If plotted, the typical force plateau behavior of the superelastic NiTi archwire now gives way to a slope. This study established regression models for estimating the magnitude of forces released by NiTi archwire when bent at various settings in an orthodontic bracket system. Four bending settings parameters were considered: archwire geometry, inter bracket distance, the magnitude of archwire deflection, and testing temperature. The relationships between the settings and the wire forces were investigated using a response surface methodology approach based on data obtained from bending simulation. The magnitude and slope of the unloading force of superelastic NiTi archwire decrease gradually as the amount of wire deflection and inter-bracket distance increase, respectively. NiTi archwires with a diameter of 0.016 inches are best used in the early stages of orthodontic therapy because of their lower unloading forces of 0.57 N to 1.71 N and lower force slope values of 0.13 N/mm to 0.72 N/mm. The developed regression models have strong R-squared values

### ARTICLE INFO

#### *Article history:*

Received: 21 January 2022

Accepted: 29 March 2022

Published: 21 July 2022

DOI: <https://doi.org/10.47836/pjst.30.4.04>

#### *E-mail addresses:*

sarehaiman@usm.my (Sareh Aiman Hilmi Abu Seman)  
chingwei90@hotmail.com (Ching Wei Ng)  
mefauzinizam@usm.my (Muhammad Fauzinizam Razali)  
abdus@usm.my (Abdus Samad Mahmud)

\* Corresponding author

for the loading force, unloading force, and force slope of 0.996, 0.9830, and 0.9748, respectively, and may thus be used to aid the orthodontist in forecasting the amount of force being exerted on a tooth in various malocclusion conditions.

**Keywords:** Bending, NiTi archwire, orthodontic bracket, response surface methodology, unloading force

## INTRODUCTION

Fixed appliance therapy is one of the orthodontic options available to treat malocclusions, as it encourages correct tooth alignment and overall facial esthetics (Papageorgiou et al., 2017). The fixed appliance is installed by attaching an orthodontic bracket on every tooth with adhesive, followed by carefully inserting an archwire into the bracket slot. This insertion procedure usually induces localized bending along the wire length due to the bracket's irregular position as a result of the tooth's malocclusion. The archwire is then secured inside the bracket slot using elastomeric ligatures, fine wires, or a metal door, depending on the bracket's ligation type considered for the treatment. As the orthodontic archwire attempts to restore its original straight form during the therapy, the malposed tooth is gradually pushed upwards or downwards, depending on the direction of bending recovery of the archwire.

In order to accurately anticipate the tooth movement, the magnitude of the force exerted by the bent wire on the tooth must be within the suggested range. Many variables that influence tooth movement, such as the remodeling of tissues and bone concerning the applied orthodontic pressure, are uncontrollable. Contrarily, the force being applied to the tooth is a controlled variable, and sufficient knowledge of the physics behind the force delivery mechanism may aid in minimizing undesired tooth movement. The recommended orthodontic forces often suggested, ranging from 0.10 N to 1.20 N (Wu et al., 2018; Theodorou et al., 2019), are regarded as the optimum force levels for a speedier and more comfortable treatment experience.

Nickel-titanium (NiTi) orthodontic archwire is commonly selected in orthodontic treatment as it can deliver light and continuous force during bending, which promotes tooth movement. However, it is reported that in orthodontic bracket configurations, friction modifies the constant force behavior of superelastic NiTi archwire to a slope (Nucera et al., 2014; Razali et al., 2018). The friction intensity encountered by NiTi archwire as it slides within the bracket slot could also be affected by the distance set between brackets, a vertical discrepancy of bracket placement, oral temperature, wire sizes, and ligating type used to secure the archwire (Kusy & Whitley, 2000; Higa et al., 2017). While the friction component is unavoidable, the bending settings are adjustable and could be controlled to minimize the deviation of the wire force from the optimal force levels. The work aimed to establish regression models for anticipating the forces produced by a NiTi archwire when bent in various orthodontic bracket systems. The magnitude of the archwire force was determined at different bending settings using a three-dimensional finite-element model of wire bending in a three-bracket configuration. The bending settings considered were the archwire geometry, the inter bracket distance, the magnitude of archwire deflection, and the testing temperature. The wire force regression models were built using the response surface methodology approach. In the future, this regression model may enable the orthodontist to

anticipate the NiTi archwire force early in the treatment process, regardless of the patient's malocclusion state.

## MATERIALS AND METHODS

The force-deflection data of the NiTi archwires in an orthodontic bracket configuration were determined using the three-dimensional finite element model developed in our earlier work (Razali et al., 2018). The model considered the bending of a single superelastic NiTi wire in a three-bracket configuration and has been validated against experimental work. The model was developed using Abaqus 6.12.2 software. A user material subroutine (UMAT/Nitinol) developed by Auricchio and Taylor (1997) was employed to assign the superelastic behavior of NiTi alloy on the archwire model.

The half-cut view of the developed three-dimensional finite element model is shown in Figure 1. A bilinear rigid quadrilateral element (R3D4) was used to create three orthodontic brackets with a slot dimension of 0.46 mm (height), 2.8 mm (length), and 0.63 mm (width). The bracket slot's dimensions were determined directly from scanning electron microscopy images. A total of 6,496 elements were employed to model each bracket instance. These brackets were symmetrically positioned by spacing their midpoints apart by 7.5 mm. The middle bracket was displaced downward by 0.06 mm compared to the adjacent bracket. Therefore, it is critical to remove the space between the archwire and the middle bracket's top surface prior to initiating the bending. On the other hand, two NiTi archwire of 0.016 x 0.022-inch and 0.016-inch size with a length of 30 mm was considered in this study. Mesh was applied to the wire model using eight-node linear brick elements with reduced integration (C3D8R). For the round and rectangular wire instances, 72,000 and 72,144 elements were utilized, respectively.

The bending simulation of the superelastic NiTi wire in the bracket system is divided into two stages: loading and unloading. These steps characterize the archwire's

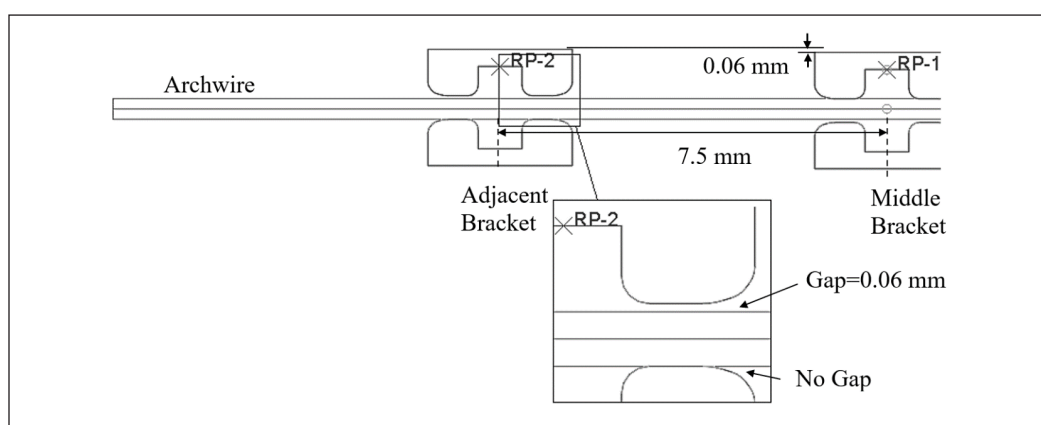


Figure 1. Positioning of archwire and brackets during the assembly stage

deformation and recovery in terms of the application and removal of the bending load, which is accomplished by downwards, and upwards displacement of the middle bracket at a displacement rate of 0.016 mm/s. The initial time increment was set to 0.01 seconds for both steps, with the minimum and maximum permissible time increments set to 0.00001 and 0.1 seconds, respectively. Only the y-axis of the middle bracket was permitted to move, while the other degree of freedom was set to zero. In addition, all degrees of freedom of the adjacent brackets were set to zero to prevent movement throughout the bending course. No boundary conditions were assigned to the wire instance, allowing the wire to move while bending freely. The oral temperature of 36°C was used as the constant for the bending environment.

This study defined the contact behavior between the wire and bracket surfaces using surface-to-surface discretization. The bracket's surface was designated the master surface, while the wire's surface was designated the slave surface. In this master-slave method, every slave node search for the nearest point on the master surface, and the contact direction is always normal to the master surface. The surface-to-surface discretization between the archwire and bracket surfaces was described using two interaction properties: normal and tangential behavior. The coefficient of friction was set at 0.27 between the NiTi archwire and the stainless-steel bracket surfaces (Thalman, 2008).

The archwire's force-deflection behavior during bending was determined using the vertical response force (RF2) and displacement (U2) acquired from the middle bracket reference point (RP-1). As shown in Figure 2, three force criteria were obtained from the force-deflection curve to create the force regression model. First, the loading force

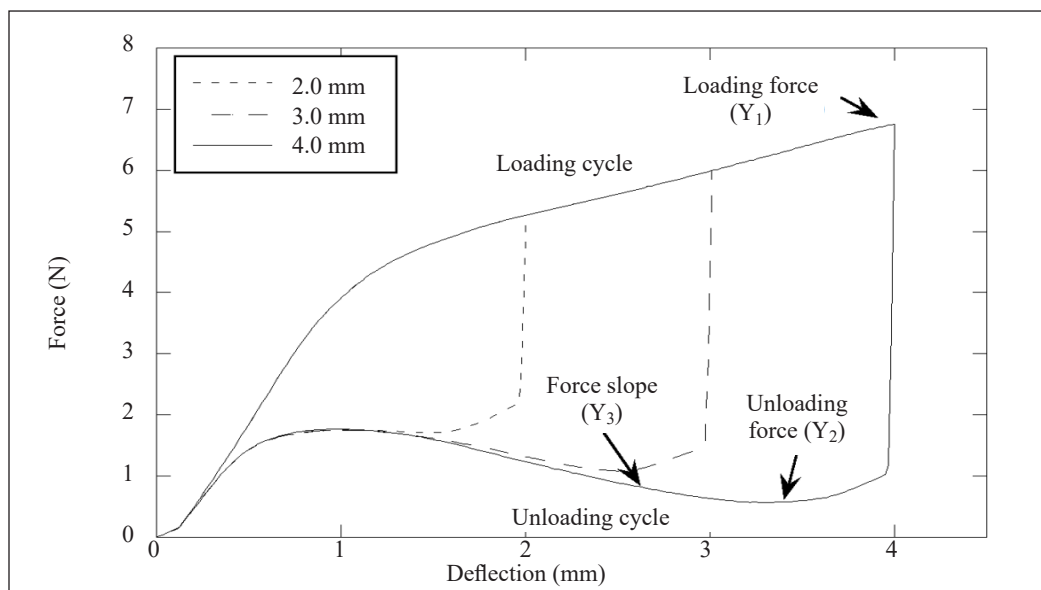


Figure 2. Force-deflection behavior of the NiTi archwire bent at different deflection magnitudes

is determined at the maximum deflection applied on the wire. This response denotes the force the patient experienced upon the NiTi wire installation on the bracket. First, the unloading force is determined when the bracket was deactivated by 0.8 mm from the loading deflection, and this response shows the force transmitted from the archwire to the malposed tooth with the least magnitude. Meanwhile, the slope was calculated using the unloading curve's best linear section. This parameter signifies the rate of changes recorded in the force magnitude as the wire recovered during the unloading cycle.

A statistical design of experiments (DOE) was created using the central composite design (CCD), a tool for designing response surface models. In summary, the design utilizes three types of design points: two-level factorial ( $2^k$ ), axial points ( $2^k$ ), and center points. The central composite design method is used to fit and estimate the coefficients of a second-order equation. Equation 1 illustrates the standard form of this second-order equation model with two factors.

$$Y = \beta_0 + \sum_{i=1}^k \beta_i X_i + \sum_{i=1}^k \beta_{ii} X_i^2 + \sum_{i=1}^{k-1} \sum_{j=i+1}^k \beta_{ij} X_i X_j + \varepsilon \quad [1]$$

where  $Y$  is the response of interest,  $\beta_0$  is a constant coefficient,  $\beta_i$ ,  $\beta_{ii}$ , and  $\beta_{ij}$  are the interaction coefficients of the linear, the quadratic, and the second-order terms, respectively.  $X_i$  and  $X_j$  are the factors,  $k$  is the number of studied factors, and  $\varepsilon$  is the random error.

As detailed in Table 1, each of the statistical model's bending settings (factors) has three levels, denoted mathematically by minus one (-1), zero (0), and plus one (+1). The inter-bracket distance, wire deflection, and testing temperature varied between 7.0 mm and 8.0 mm, 2.0 mm and 4.0 mm, and 26°C to 46°C, respectively. These factors were taken into account in this study to account for the variance in wire-bracket placement and oral condition found between patients, and the ranges for each factor were drawn from the literature (Nucera et al., 2014; Franchi et al., 2009; Elayyan et al., 2010; Badawi et al., 2009; Arreghini et al., 2016; Alavi & Hosseini, 2012; Wilkinson et al., 2002). The amount

Table 1  
*Actual and coded values for each central composite design factor*

| Numeric Factor (symbol)            | Coded Value |             |    |
|------------------------------------|-------------|-------------|----|
|                                    | -1          | 0           | 1  |
| Actual Value                       |             |             |    |
| Inter-bracket distance, mm ( $A$ ) | 7           | 7.5         | 8  |
| Wire deflection, mm ( $B$ )        | 2           | 3           | 4  |
| Testing temperature, °C ( $C$ )    | 26          | 36          | 46 |
| Coded Value                        |             |             |    |
| Categoric Factor (symbol)          |             |             |    |
| Geometry ( $D$ )                   | Round       | Rectangular |    |
|                                    | {1}         | {-1}        |    |

of the wire deflection of 1.0 mm was omitted from this investigation due to its linear force-deflection characteristic, which is typical in common alloys (Thalman, 2008).

The design included two categorical factors: round and rectangular wire geometry. A total of forty simulation runs were carried out with reference to the following equation  $CCD = (2^k + 2k + R)*L$ , where  $k$  is the number of factors,  $R$  is the number of replications at the design center, and  $L$  is the level of the categorical factors. Each simulation took fifteen hours to finish on a 2.67GHz CPU with a 24-GB memory.

## RESULTS

The magnitudes of the forces obtained from the simulation of archwire bending at different configurations are summarized in Table 2, which lists the possible combination of bending conditions designed by the central composite design (CCD). As can be observed, the loading and unloading forces ranged between 4.08 N and 18.20 N and 0 N and 4.72 N, respectively. On the other hand, the force slope varied between 0.00 N/mm and 2.72 N/mm. Notably, run 30 is the most critical bending condition (combination of 7.0 mm inter-bracket distance, 4.0 mm wire deflection, and 46°C testing temperature) since it has the highest loading force magnitude of 18.20 N. Additionally, it is noteworthy that the rectangular wire's unloading force was zero for running 4, where the wire was deflected to 4.0 mm in 26°C environments with the brackets distanced at 7.0 mm in between. The zero-newton force demonstrated that the wire's unloading force had weakened to zero as it slid along the bracket slot in a high friction condition. However, this zero-newton force was not recorded when the wire's temperature reached 46°C. It is due to the superelastic NiTi wire strengthening at greater temperatures, where the enhanced unloading force aids in overcoming the sliding friction.

The regression models for the archwire force prediction were generated using Design Expert (Version 7.0, Trial Version) software. The best-fitting models, with probability values ( $Prob > F$ ) of less than 0.0001, were obtained by selecting a quadratic model for the loading force ( $Y_1$ ), the unloading force ( $Y_2$ ), and the force slope ( $Y_3$ ). The final regression models, in terms of the coded factors, are as in Equations 2-4:

$$Y_1 = 9.59 - 1.10A + 1.21B + 1.17C - 3.57D - 0.11AB - 0.056AC + 0.42AD + 0.067BC - 0.48BD - 0.42CD \quad [2]$$

$$Y_2 = 1.63 + 0.050A - 1.03B + 0.37C - 0.56D + 0.28AB - 0.22BC + 0.41BD - 0.13CD \quad [3]$$

$$Y_3 = 1.00 - 0.31A - 0.50B + 0.19C - 0.36D - 0.083AB - 0.063AC + 0.12AD - 0.18BD - 0.069CD - 0.21B^2 \quad [4]$$

where A, B, C, and D are the factors of Table 1.

Table 2  
*Summary of the force data obtained from the simulated force-deflection curves*

| Run | Factor (Coded)            |                     |                 |                   | Response (Y)       |                      |                     |                    |                      |                     |
|-----|---------------------------|---------------------|-----------------|-------------------|--------------------|----------------------|---------------------|--------------------|----------------------|---------------------|
|     | Interbracket Distance (A) | Wire Deflection (B) | Temperature (C) | Wire Geometry (D) | Simulation         |                      |                     | Prediction         |                      |                     |
|     |                           |                     |                 |                   | Loading Force, (N) | Unloading Force, (N) | Force Slope, (N/mm) | Loading Force, (N) | Unloading Force, (N) | Force Slope, (N/mm) |
| 1   | 1                         | 1                   | 1               | {1}               | 6.82               | 0.73                 | 0.69                | 6.78               | 0.80                 | 0.61                |
| 2   | 1                         | -1                  | 1               | {1}               | 5.33               | 1.91                 | 0.00                | 5.34               | 1.84                 | 0.02                |
| 3   | 1                         | 0                   | 0               | {-1}              | 11.73              | 2.17                 | 1.07                | 11.75              | 2.29                 | 0.89                |
| 4   | -1                        | 1                   | -1              | {-1}              | 14.77              | 0.00                 | 2.19                | 14.79              | -0.11                | 1.84                |
| 5   | 0                         | -1                  | 0               | {-1}              | 11.30              | 3.61                 | 0.44                | 11.40              | 3.65                 | 0.37                |
| 6   | 1                         | -1                  | -1              | {-1}              | 8.77               | 2.55                 | 0.04                | 8.68               | 2.74                 | 0.05                |
| 7   | -1                        | 1                   | -1              | {1}               | 6.67               | 0.13                 | 0.86                | 6.65               | 0.07                 | 0.80                |
| 8   | 0                         | 0                   | 0               | {1}               | 6.00               | 1.08                 | 0.62                | 5.99               | 1.07                 | 0.62                |
| 9   | 0                         | 0                   | 0               | {-1}              | 13.16              | 2.22                 | 1.40                | 13.18              | 2.17                 | 1.36                |
| 10  | 0                         | 0                   | 0               | {-1}              | 13.16              | 2.22                 | 1.40                | 13.18              | 2.17                 | 1.36                |
| 11  | 1                         | -1                  | -1              | {1}               | 4.08               | 1.20                 | 0.00                | 4.08               | 0.98                 | 0.00                |
| 12  | 0                         | 0                   | 0               | {1}               | 6.00               | 1.08                 | 0.62                | 5.99               | 1.07                 | 0.62                |
| 13  | -1                        | 0                   | 0               | {-1}              | 14.93              | 2.36                 | 1.66                | 14.91              | 2.04                 | 1.94                |
| 14  | 0.                        | 0                   | 0               | {-1}              | 13.16              | 2.22                 | 1.40                | 13.18              | 2.17                 | 1.36                |
| 15  | 0                         | 1                   | 0               | {1}               | 6.75               | 0.57                 | 0.68                | 6.73               | 0.45                 | 0.75                |
| 16  | 1                         | 1                   | -1              | {-1}              | 11.49              | 0.87                 | 0.99                | 11.58              | 0.79                 | 1.09                |
| 17  | 0                         | 0                   | 0               | {1}               | 6.00               | 1.08                 | 0.62                | 5.99               | 1.07                 | 0.62                |
| 18  | -1                        | -1                  | 1               | {1}               | 6.71               | 2.23                 | 0.47                | 6.67               | 2.44                 | 0.40                |
| 19  | 0                         | 1                   | 0               | {-1}              | 14.88              | 1.11                 | 1.48                | 14.83              | 0.69                 | 1.77                |
| 20  | 0                         | 0                   | 0               | {1}               | 6.00               | 1.08                 | 0.62                | 5.99               | 1.07                 | 0.62                |
| 21  | 1                         | -1                  | 1               | {-1}              | 11.55              | 4.11                 | 0.15                | 11.53              | 4.20                 | 0.19                |
| 22  | 0                         | -1                  | 0               | {1}               | 5.28               | 1.71                 | 0.13                | 5.26               | 1.69                 | 0.09                |
| 23  | 0                         | 0                   | 0               | {-1}              | 13.16              | 2.22                 | 1.40                | 13.18              | 2.17                 | 1.36                |
| 24  | 1                         | 0                   | 0               | {1}               | 5.35               | 1.06                 | 0.47                | 5.37               | 1.09                 | 0.38                |
| 25  | 0                         | 0                   | 0               | {1}               | 6.00               | 1.08                 | 0.62                | 5.99               | 1.07                 | 0.62                |
| 26  | 0                         | 0                   | 1               | {-1}              | 14.72              | 2.70                 | 1.71                | 14.69              | 2.72                 | 1.68                |
| 27  | -1                        | -1                  | -1              | {1}               | 5.14               | 1.41                 | 0.19                | 5.16               | 1.53                 | 0.18                |
| 28  | 1                         | 1                   | -1              | {1}               | 5.28               | 0.47                 | 0.44                | 5.27               | 0.73                 | 0.47                |
| 29  | -1                        | 0                   | 0               | {1}               | 6.80               | 1.13                 | 0.72                | 6.74               | 1.06                 | 0.93                |
| 30  | -1                        | 1                   | 1               | {-1}              | 18.20              | 0.20                 | 2.72                | 18.05              | 0.62                 | 2.73                |
| 31  | 0                         | 0                   | 0               | {1}               | 6.00               | 1.08                 | 0.62                | 5.99               | 1.07                 | 0.62                |
| 32  | 0                         | 0                   | 1               | {1}               | 6.72               | 1.31                 | 0.69                | 6.74               | 1.31                 | 0.73                |
| 33  | 0                         | 0                   | -1              | {-1}              | 11.55              | 1.68                 | 1.08                | 11.44              | 1.62                 | 1.07                |
| 34  | -1                        | 1                   | 1               | {1}               | 8.26               | 0.31                 | 1.27                | 8.37               | 0.19                 | 1.21                |
| 35  | 0                         | 0                   | 0               | {-1}              | 13.16              | 2.22                 | 1.40                | 13.18              | 2.17                 | 1.37                |
| 36  | 0                         | 0                   | -1              | {1}               | 5.22               | 0.84                 | 0.46                | 5.23               | 0.83                 | 0.49                |
| 37  | -1                        | -1                  | 1               | {-1}              | 14.44              | 4.72                 | 1.14                | 14.46              | 4.59                 | 1.07                |
| 38  | -1                        | -1                  | -1              | {-1}              | 11.22              | 3.02                 | 0.42                | 11.23              | 3.07                 | 0.51                |
| 39  | 0                         | 0                   | 0               | {-1}              | 13.16              | 2.22                 | 1.40                | 13.18              | 2.17                 | 1.37                |
| 40  | 1                         | 1                   | 1               | {-1}              | 14.83              | 1.44                 | 1.56                | 14.81              | 1.46                 | 1.55                |

The results from the analysis of variance (ANOVA) of each regression model are summarized in Table 3. The coefficient of determination (R-squared) is the variable of interest in this statistical analysis, which determines how well the regression line fits the simulated force data from the bending simulations. Higher R-squared values indicate that

Table 3

*Summary of ANOVA for the loading force ( $Y_1$ ), the unloading force ( $Y_2$ ), and the force slope ( $Y_3$ )*

| Source  | Sum of Squares | DF | Mean Square            | F Value   | Prob > F |
|---|----------------|----|------------------------|-----------|----------|
| <b>ANOVA for Response Surface Quadratic model</b> |                |    |                        |           |          |
| Model ( $Y_1$ )                                   | 603.35         | 10 | 60.33                  | 7771.79   | < 0.0001 |
| <i>A</i> -Inter-bracket Distance                  | 24.00          | 1  | 24.00                  | 3091.79   | < 0.0001 |
| <i>B</i> -Deflection                              | 29.11          | 1  | 29.11                  | 3750.07   | < 0.0001 |
| <i>C</i> -Temperature                             | 27.35          | 1  | 27.35                  | 3523.59   | < 0.0001 |
| <i>D</i> -Wire Geometry                           | 510.72         | 1  | 510.72                 | 65787.26  | < 0.0001 |
| <i>AB</i>   | 0.18           | 1  | 0.18                   | 23.27     | < 0.0001 |
| <i>AC</i>   | 0.051          | 1  | 0.051                  | 6.52      | 0.0162   |
| <i>AD</i>   | 3.59           | 1  | 3.59                   | 462.05    | < 0.0001 |
| <i>BC</i>   | 0.073          | 1  | 0.073                  | 9.39      | 0.0047   |
| <i>BD</i>   | 4.66           | 1  | 4.66                   | 599.76    | < 0.0001 |
| <i>CD</i>   | 3.60           | 1  | 3.60                   | 464.24    | < 0.0001 |
| Residual  | 0.23           | 29 | $7.763 \times 10^{-3}$ |           |          |
| Lack of Fit                                       | 0.23           | 19 | 0.012                  |           |          |
| Pure Error  | 0.000          | 10 | 0.000                  |           |          |
| Std. Dev.   | 0.088          |    |                        | R-Squared | 0.9996   |
| Mean  | 9.59           |    |                        | C.V. %    | 0.92     |
| <b>ANOVA for Response Surface Quadratic model</b> |                |    |                        |           |          |
| Model ( $Y_2$ )                                   | 42.37          | 8  | 5.30                   | 223.58    | < 0.0001 |
| <i>A</i> -Inter-bracket Distance                  | 0.050          | 1  | 0.050                  | 2.11      | 0.1563   |
| <i>B</i> -Deflection                              | 21.30          | 1  | 21.30                  | 899.10    | < 0.0001 |
| <i>C</i> -Temperature                             | 2.81           | 1  | 2.81                   | 118.40    | < 0.0001 |
| <i>D</i> -Wire Geometry                           | 12.51          | 1  | 12.51                  | 528.07    | < 0.0001 |
| <i>AB</i>   | 1.25           | 1  | 1.25                   | 52.95     | < 0.0001 |
| <i>BC</i>   | 0.80           | 1  | 0.80                   | 33.81     | 0.0001   |
| <i>BD</i>   | 3.31           | 1  | 3.31                   | 139.84    | < 0.0001 |
| <i>CD</i>   | 0.34           | 1  | 0.34                   | 14.38     | 0.0006   |
| Residual  | 0.73           | 29 | 0.024                  |           |          |
| Lack of Fit                                       | 0.73           | 19 | 0.035                  |           |          |
| Pure Error  | 0.00           | 10 | 0.00                   |           |          |
| Std. Dev.   | 0.15           |    |                        | R-Squared | 0.9830   |
| Mean  | 1.63           |    |                        | C.V. %    | 9.42     |

Table 3 (*continue*)

| Source  | Sum of Squares | DF | Mean Square | F Value | Prob > F |
|---|----------------|----|-------------|---------|----------|
| <b>ANOVA for Response Surface Quadratic model</b> |                |    |             |         |          |
| Model ( $Y_3$ )                                   | 14.25          | 10 | 1.43        | 112.21  | < 0.0001 |
| <i>A</i> -Inter-bracket Distance                  | 1.94           | 1  | 1.94        | 152.77  | < 0.0001 |
| <i>B</i> -Deflection                              | 4.90           | 1  | 4.90        | 385.76  | < 0.0001 |
| <i>C</i> -Temperature                             | 0.70           | 1  | 0.70        | 54.76   | < 0.0001 |
| <i>D</i> -Wire Geometry                           | 5.08           | 1  | 5.08        | 400.18  | < 0.0001 |
| <i>AB</i>   | 0.11           | 1  | 0.11        | 8.70    | 0.0062   |
| <i>AC</i>   | 0.064          | 1  | 0.064       | 5.02    | < 0.0001 |
| <i>AD</i>   | 0.29           | 1  | 0.29        | 22.86   | < 0.0001 |
| <i>BD</i>   | 0.65           | 1  | 0.65        | 51.01   | < 0.0001 |
| <i>CD</i>   | 0.097          | 1  | 0.097       | 7.60    | 0.0100   |
| <i>B</i> <sup>2</sup>                             | 0.42           | 1  | 0.42        | 33.41   | < 0.0001 |
| Residual  | 0.37           | 29 | 0.013       |         |          |
| Lack of Fit                                       | 0.37           | 19 | 0.019       |         |          |
| Pure Error  | 0.000          | 10 | 0.000       |         |          |
| Std. Dev.   | 0.11           |    | R-Squared   | 0.9748  |          |
| Mean  | 0.90           |    | C.V. %      | 12.58   |          |

the model correctly predicts the archwire force within the range of factors studied. The ANOVA analysis reveals that the R-squared values for the loading force ( $Y_1$ ), the unloading force ( $Y_2$ ), and the force slope ( $Y_3$ ) are 0.996, 0.9830, and 0.9748, respectively, proving that the chosen quadratic models are good response predictors and are in agreement with the actual simulation results. Additionally, the probability values (Prob>F) are less than 0.0001, indicating the significance of the developed prediction equations.

Given that three factors influence the force responses, a perturbation plot is used to determine which factors have the greatest effect on the wire forces. Each factor's reference point (coded as 0) is set to the midpoint by default in the program's settings. A line plot with a high inclination or curvature indicates that the response is sensitive to changes in a particular factor. In contrast, a line plot with a relatively flat slope indicates that the response is insensitive to that factor.

The loading force perturbation plots for the rectangular and round archwire are shown in Figures 3(a) and 3(b), respectively. The coded values for each factor correspond to the actual values, as stated in Table 1. In brief, the loading force is highly dependent on the wire's geometry, with rectangular wire always releasing greater force magnitude. For example, the rectangular wire's forces ranged from 11.30 N to 14.93 N. However, the values decrease dramatically as soon as the round wire is used, now ranging from 5.22 N to 6.80 N. Bear in mind that while both archwires release greater forces than the suggested

values, their severe impact on dentition may be of some concern, as the force strength decrease abruptly to a lower magnitude of 0.55 N as soon as small tooth movement takes place by 0.5 mm as seen in Figure 2.

Figures 3(a) and 3(b) demonstrate that all considered factors have similar significance on the loading force magnitude. The loading force increased linearly with increasing wire deflection and temperature while linearly decreasing as the inter-bracket distance increased. It is seen that similar plot trends are observed for both wire geometries, with the rectangular wire exhibiting the steepest slope. It demonstrates that the rectangular wire magnifies the impact of bending factors on the wire force. For comparison, at a given temperature of 36°C and deflection of 3.0 mm, the change of inter-bracket distance from 7.0 mm to 8.0 mm significantly decreased the rectangular wire's loading force by 3.20 N (from 14.93 N to 11.73 N). Meanwhile, a smaller loading force reduction of 1.45 N (from 6.80 N to 5.35 N) was recorded when the round wire was considered for the same bending settings.

The unloading force perturbation plots for the rectangular and round archwire are shown in Figures 4(a) and 4(b), respectively. The rectangular wire's unloading forces ranged between 1.11 N and 3.61 N. In contrast, the round wire's unloading forces ranged between 0.57 N and 1.71 N. The plots demonstrate that the unloading force is the most responsive to variations in wire deflection, followed by changes in temperature and inter-bracket distance. It is noticed that both wire geometries exhibit similar plot patterns, with the rectangular wire demonstrating the biggest variations in force magnitudes as a function of bending factor variation. The unloading force magnitude decreased significantly with increasing wire deflection and mildly increased as the temperature and the inter-bracket distance increased. For instance, at a given temperature of 36°C and inter-bracket distance

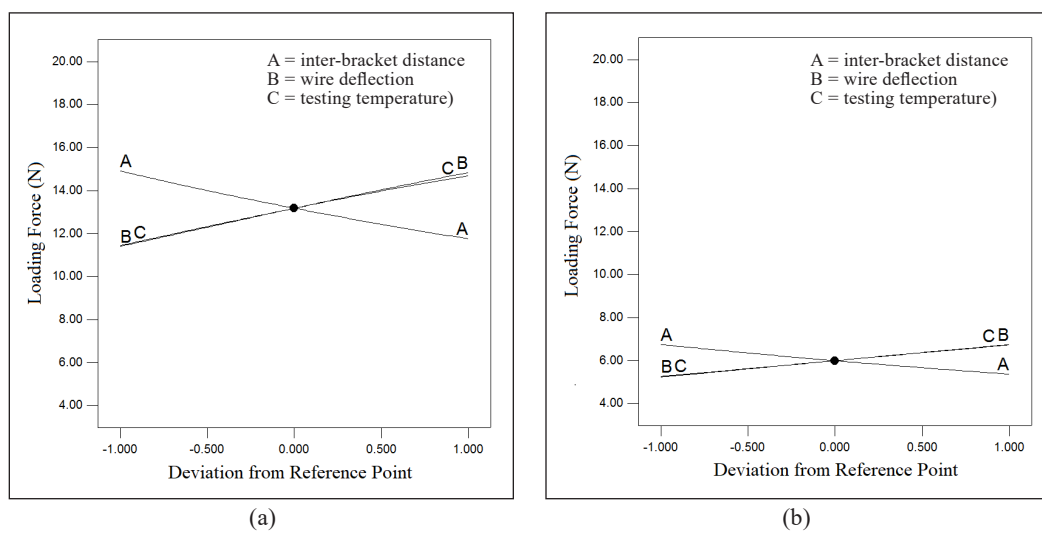


Figure 3. Perturbation plot showing the effect of factors on the loading force of (a) rectangular; and (b) round archwire

of 7.5 mm, the change of wire deflection from 2.0 mm to 4.0 mm had considerably reduced the unloading force of the rectangular wire by 2.50 N (from 3.61 N to 1.11 N). Meanwhile, a smaller unloading force reduction of 1.14 N (from 1.71 N to 0.57 N) was recorded using round wire for the same bending settings.

The wire force slope perturbation plots for the rectangular and round archwire are shown in Figures 5(a) and 5(b), respectively. The rectangular wire had a force slope of

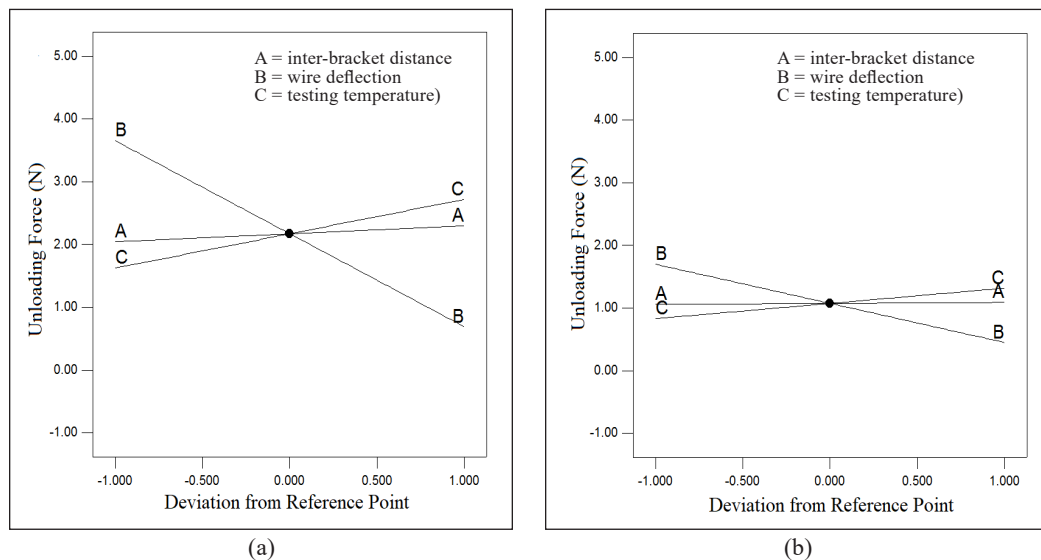


Figure 4. Perturbation plots showing the effect of factors on the unloading force of (a) rectangular; and (b) round archwire

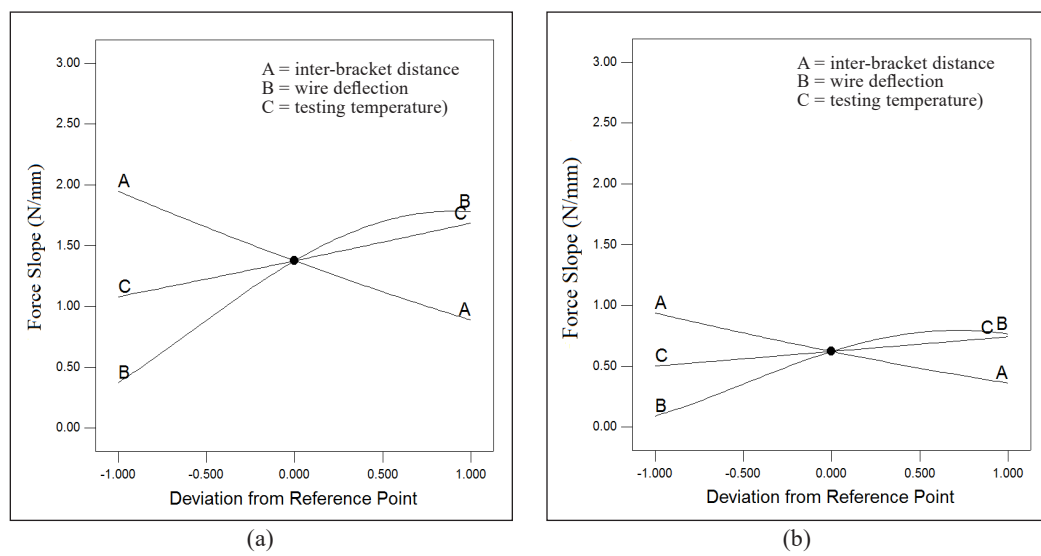


Figure 5. Perturbation plots showing the effect of factors on the force slope of (a) rectangular; and (b) round archwire

0.44 N/mm to 1.71 N/mm, whereas the round wire had a force slope of 0.13 N/mm to 0.72 N/mm. In general, the force slope is the most sensitive to changes in the amount of wire deflection, followed by the changes in inter-bracket distance and temperature. The plots also demonstrate that the force slope is directly proportional to the wire deflection and the bending temperature but inversely proportional to the distance set between brackets. It is interesting to highlight that the force slope's sensitivity to the deflection is reduced as the wire deflects more than 3.0 mm. Both wire geometries demonstrate similar plot trends, with the rectangular wire having the highest change in force slope values when bending settings are varied. For example, at a given temperature of 36°C and deflection of 3.0 mm, the change of inter-bracket distance from 7.0 mm to 8.0 mm had reduced the force slope of the rectangular wire by 0.59 N/mm (from 1.66 N/mm to 1.07 N/mm). Meanwhile, a smaller force slope reduction of 0.25 N/mm (from 0.72 N/mm to 0.47 N/mm) was recorded using round wire for the same bending settings.

## DISCUSSION

It is difficult to precisely estimate the archwire force during orthodontic treatment due to many uncontrolled variables affecting the force transmission, such as the pressure from the lips and tongue and the biting force (Proffit et al., 2018). Therefore, while utilizing the established regression models, readers should remember that the estimated biomechanical forces are only valid for the wire-bracket combination and settings addressed in this work. In addition, the choice of ligation methods may result in varying degrees of frictional resistance, thus further complicating the force prediction. For instance, when the elastomeric ligatures are considered during the orthodontic treatment, the overall resistance experienced during the sliding is increased. As a result, the loading and unloading forces measured during the bending would rise and drop in magnitudes greater than those observed in the current study.

The goal of using a rectangular wire as soon as feasible is critical to improving tooth movement as it promotes torque control to the malposed tooth. Unfortunately, the force values summarized in Table 2 called into question the usefulness of considering the rectangular wire at the early stage of leveling since the force magnitudes vary between 1.44 N and 4.72 N for all the considered bending settings, exceeding the ideal force range. Based on this observation, orthodontists are encouraged to avoid using rectangular wires in scenarios involving persistently significant tooth level discrepancy. On the contrary, using the 0.016-inch round archwire would be the optimal choice, as the force varied between 0.13 N and 0.73 N for the large 4.0 mm deflection condition. Notably, this force range is within the reported range of 0.10 N to 1.20 N for optimal tooth movement (Wu et al., 2018; Theodorou et al., 2019).

The relationship between the archwire force and the amount of bending deflection applied to the wire may provide an advantage during orthodontic treatment, specifically during the reactivation process. The present finding of increased wire force at smaller wire deflection suggests that the NiTi archwire may be momentarily removed and then reinstalled during the clinical visit to release more force than at initial activation. For example, if a tooth has traveled away from its original vertical discrepancy of 4.0 mm, reactivating the same wire at a lesser discrepancy, say 2.0 mm, may result in a higher unloading force being delivered. This greater force may be advantageous for leveling a tooth of bigger size, such as a premolar or molar teeth. Additionally, the force data in Table 2 also demonstrate that the unloading force increases as the oral temperature increases. The NiTi wire stiffens when a patient consumes warm drinks, and the unloading force magnitude increases abruptly.

For healthier tooth movement, the force released by the archwire to the dentition must be light and steady throughout the therapy. Therefore, maintaining the periodontal ligament's present cellular activity is necessary for connection to an optimal tooth movement experience. From Table 2, there was only one configuration in which the NiTi wire in the bracket system produced consistent force magnitude during the unloading cycle. This configuration, which incorporates a 2.0 mm wire deflection in 8.0 mm inter-bracket distance condition, results in a force slope of practically zero throughout the unloading cycle. In comparison, at the critical bending conditions, the round and rectangular wire exhibited a steeper force slope of 1.27 N/mm and 2.72 N/mm, respectively.

Given that leveling treatment is usually associated with significant tooth misalignment, the optimal strategy would be to utilize a springier archwire to reduce the effect of sliding friction on the amount and slope of the unloading force. The tiniest round archwire currently available on the market measures 0.012 inches in diameter. According to the expanded simulation work utilizing a comparable three-dimensional finite element model, the unloading of the 0.012-inch superelastic NiTi wire from 4.0 mm deflection in a 36°C environment demonstrated an unloading force slope of 0.3 N/mm (Razali, 2018). This force changing rate is significantly smaller than the rate exhibited by the 0.016 × 0.022-inch and 0.016-inch wires considered in this study, which had a force slope of 1.48 N/mm and 0.68 N/mm, respectively.

## CONCLUSION

Three regression models for predicting the loading, unloading, and slope of force exerted by a superelastic NiTi archwire in an orthodontic bracket system were successfully established using response surface methods. The developed regression models exhibit high R-squared values of 0.996, 0.9830, and 0.9748 for the loading, unloading force, and force slope, respectively. The impact of the considered bending settings on wire force is substantially stronger when the rectangular wire is used. The magnitude and slope of the unloading force

of superelastic NiTi wire decrease linearly as the amount of wire deflection and the distance between brackets increase, respectively. Therefore, the 0.016-inch diameter archwire is more appropriate for use during the early stages of orthodontic treatment due to its lighter force of 0.57 N to 1.71 N and a lower force slope of 0.13 N/mm to 0.72 N/mm. On the other hand, the use of  $0.016 \times 0.022$ -inch rectangular wire may cause patient discomfort, as the force transferred to induce tooth movement may surpass 3.61 N.

## ACKNOWLEDGEMENTS

The authors are grateful for the financial support of the Ministry of Higher Education Malaysia under the Fundamental Research Grant Scheme (FRGS/1/2020/TK0/USM/03/5).

## REFERENCES

- Alavi, S., & Hosseini, N. (2012). Load-deflection and surface properties of coated and conventional superelastic orthodontic archwires in conventional and metal-insert ceramic brackets. *Dental Research Journal*, 9(2), 133-138. <https://doi.org/10.4103/1735-3327.95225>
- Arreghini, A., Lombardo, L., Mollica, F., & Siciliani, G. (2016). Load deflection characteristics of square and rectangular archwires. *International Orthodontics*, 14(1), 1-14. <https://doi.org/10.1016/j.ortho.2015.12.011>
- Auricchio, F., & Taylor, R. L. (1997). Shape-memory alloys: Modelling and numerical simulations of the finite-strain superelastic behavior. *Computer Methods in Applied Mechanics and Engineering*, 143(1-2), 175-194. [https://doi.org/10.1016/S0045-7825\(96\)01147-4](https://doi.org/10.1016/S0045-7825(96)01147-4)
- Badawi, H. M., Toogood, R. W., Carey J. P. R., Heo, G., & Major, P. W. (2009). Three-dimensional orthodontic force measurements. *American Journal of Orthodontics and Dentofacial Orthopedics*, 136(4), 518-528. <https://doi.org/10.1016/j.ajodo.2009.02.025>
- Elayyan, F., Silikas, N., & Bearn, D. (2010). Mechanical properties of coated superelastic archwires in conventional and self-ligating orthodontic brackets. *American Journal of Orthodontics and Dentofacial Orthopedics*, 137(2), 213-217. <https://doi.org/10.1016/j.ajodo.2008.01.026>
- Franchi, L., Baccetti, T., Camporesi, M., & Giuntini, V. (2009). Forces released by nonconventional bracket or ligature systems during alignment of buccally displaced teeth. *American Journal of Orthodontics and Dentofacial Orthopedics*, 136(3), 316.e1-316.e6. <https://doi.org/10.1016/j.ajodo.2009.02.016>
- Higa, R. H., Henriques, J. F. C., Janson, G., Matias, M., Freitas, K. M. S., Henriques, F. P., & Francisconi, M. F. (2017). Force level of small diameter nickel-titanium orthodontic wires ligated with different methods. *Progress in Orthodontics*, 18(1), Article 21. <https://doi.org/10.1186/s40510-017-0175-z>
- Kusy, R. P., & Whitley, J. Q. (2000). Resistance to sliding of orthodontic appliances in the dry and wet states: Influence of archwire alloy, interbracket distance, and bracket engagement. *Journal of Biomedical Materials Research*, 52(4), 797-811. [https://doi.org/10.1002/1097-4636\(20001215\)52:4%3C797::AID-JBM25%3E3.0.CO;2-9](https://doi.org/10.1002/1097-4636(20001215)52:4%3C797::AID-JBM25%3E3.0.CO;2-9)
- Nucera, R., Gatto, E., Borsellino, C., Aceto, P., Fabiano, F., Matarese, G., Perillo, L., & Cordasco, G. (2014). Influence of bracket-slot design on the forces released by superelastic nickel-titanium alignment

- wires in different deflection configurations. *The Angle Orthodontist*, 84(3), 541-547. <https://doi.org/10.2319/060213-416.1>
- Papageorgiou, S. N., Höchli, D., & Eliades, T. (2017). Outcomes of comprehensive fixed appliance orthodontic treatment: A systematic review with meta-analysis and methodological overview. *The Korean Journal of Orthodontics*, 47(6), 401-413. <https://doi.org/10.4041/kjod.2017.47.6.401>
- Proffit, W., Fields, H., Larson, B., & Sarver, D. (2018). *Contemporary orthodontics*. Elsevier.
- Razali, M. F. (2018). *Phase transformation and force-deflection responses of NiTi archwire for bracket assembly in orthodontic treatment* [Unpublished Doctoral dissertation]. Universiti Sains Malaysia, Malaysia.
- Razali, M. F., Mahmud, A. S., & Mokhtar, N. (2018). Force delivery of NiTi orthodontic archwire at different magnitude of deflections and temperatures: A finite element study. *Journal of the Mechanical Behavior of Biomedical Materials*, 77, 234-241. <https://doi.org/10.1016/j.jmbbm.2017.09.021>
- Thalman, T. D. (2008). *Unloading behavior and potential binding of superelastic orthodontic leveling wires* [Unpublished Doctoral dissertation]. Saint Louis University, USA.
- Theodorou, C. I., Kuijpers-Jagtman, A. M., Bronkhorst, E. M., & Wagener, F. A. D. T. G. (2019). Optimal force magnitude for bodily orthodontic tooth movement with fixed appliances: A systematic review. *American Journal of Orthodontics and Dentofacial Orthopedics*, 156(5), 582-592. <https://doi.org/10.1016/j.ajodo.2019.05.011>
- Wilkinson, P. D., Dysart, P. S., Hood, J. A. A., & Herbison, G. P. (2002). Load-deflection characteristics of superelastic nickel-titanium orthodontic wires. *American Journal of Orthodontics and Dentofacial Orthopedics*, 121(5), 483-495. <https://doi.org/10.1067/mod.2002.121819>
- Wu, J., Liu, Y., Peng, W., Dong, H., & Zhang, J. (2018). A biomechanical case study on the optimal orthodontic force on the maxillary canine tooth based on finite element analysis. *Journal of Zhejiang University Science B*, 19(7), 535-546. <https://doi.org/10.1631/jzus.B1700195>

